J. Fluid Mech. (2011), *vol.* 686, *pp.* 239–249.
doi:10.1017/jfm.2011.326

Shelfbreak upwelling induced by alongshore currents: analytical and numerical results

Robert N. Miller[1,2]†, Ricardo P. Matano[1] and Elbio D. Palma[3]

[1] College of Oceanic and Atmospheric Sciences, Oregon State University, Corvallis, OR 97331-5503, USA

[2] INRIA Grenoble Rhône-Alpes, Laboratoire Jean Kuntzman, 38041 Grenoble, France

[3] Departmento de Fisica, Universidad Nacional del Sur and Instituto Argentino de Oceanografia (CONICET), 8000, Bahia Blanca, Argentina

(Received 4 February 2011; revised 6 May 2011; accepted 26 July 2011; first published online 23 September 2011)

Alongshore flow in the direction of propagation of coastal trapped waves can result in upwelling at the shelfbreak. The intensity of this upwelling can be comparable in magnitude to wind-driven coastal upwelling, with its associated ecological features. Recent numerical experiments by Matano & Palma indicate that this upwelling results from convergence of Ekman transport at the shelfbreak. The mechanism for this phenomenon can be understood in terms of steady solutions to the shallow water equations in the presence of Coriolis force and bottom drag. Matano & Palma interpreted their numerical results in terms of the arrested topographic wave, but did not present direct comparisons. Here we present a family of analytical solutions to the equations of the arrested topographic wave that shows striking quantitative agreement with earlier numerical results.

Key words: ocean processes, shallow water flows, topographic effects

1. Introduction

The fundamental physical basis for understanding upwelling at the shelfbreak in the case in which a steady alongshore current flows in the direction of the coastal trapped waves is the arrested topographic wave (Csanady 1978). The spreading of the inflow jet results in an alongshore gradient in sea surface height, which, in turn, results in a cross-shore current that is partly geostrophically balanced. Mass balance is maintained by cross-shore Ekman transport in the bottom boundary layer. Rapid change in the Ekman transport at the shelfbreak results in upwelling. Recently, Matano & Palma (2008) (hereafter MP08) performed a series of numerical experiments in which they used the Princeton Ocean Model (Blumberg & Mellor 1987) to investigate this phenomenon. A schematic diagram of the upwelling process appears in figure 2 of MP08.

Matano & Palma described their results qualitatively in terms of the arrested topographic wave, but did not present quantitative comparisons between their model results and the values predicted by the arrested topographic wave. Here we exhibit a family of analytic solutions to the equations of the arrested topographic wave. We

† Email address for correspondence: miller@coas.oregonstate.edu

focus on the case investigated by Hill (1995), in which there is no inflow on the shelf. Hill (1995) derived his solution in the course of investigating the onshore intrusions of a slope current. He did not show the solution for the slope, nor did he relate his solution to the generation of shelfbreak upwelling. We also present a generalization to a two-parameter family of inflow conditions with inflow on the shelf. Our results agree remarkably well with the numerical results of MP08. Most of the features of the output of the model of the fully stratified, nonlinear ocean can be reproduced quantitatively with this relatively simple analytical calculation.

Chapman (1986) used a linearized shallow water model similar to the one used here to study the formation of the shelf/slope front in the middle Atlantic bight. He justified the use of a vertically homogeneous model by citing observational evidence that salinity and density gradients in the middle Atlantic bight tend to compensate in a fashion that reduces cross-shelf density contrast, and therefore hypothesized that density may act like a passive tracer in this context. In his calculations, he imposed an upstream boundary condition with inflow confined to a region on the shelf inshore of the shelfbreak. His solutions were characterized by convergence of the flow, and therefore downwelling. He did not comment on the vertical structure of the flow, but his solutions, in agreement with ours, exhibit convergent flow at the shelfbreak, and hence downwelling, in the case of an imposed upstream boundary condition with flow confined to the shelf.

Gawarkiewicz & Chapman (1991) performed an experiment with a three-dimensional unstratified linearized primitive equation model coupled to an advection–diffusion model of tracer concentrations. They described three-dimensional tracer distributions, but did not show explicit three-dimensional circulation results. Like Chapman (1986), they were interested in the density front in the middle Atlantic bight, and their upstream boundary condition did not include flow on the slope.

2. The arrested topographic wave

We write the steady linearized shallow water equations on the f-plane with Rayleigh friction:

$$g\eta_x - fv = -ru/h, \tag{2.1}$$

$$g\eta_y + fu = -rv/h, \tag{2.2}$$

$$(hu)_x + (hv)_y = 0, \tag{2.3}$$

where u and v are the horizontal velocity components, η is the surface height anomaly, fu is the Coriolis acceleration, h is the depth of the undisturbed fluid and r is the coefficient of linear friction. Subscripts denote partial differentiation. Consider the case of northward flow in the southern hemisphere. Our domain extends eastward from a north–south oriented coastline. We assume a simple geometry, with topography independent of the alongshore (y) coordinate, and constant bottom slopes on the shelf and offshore of the shelfbreak.

Given cross-shore and alongshore length scales L_x and L_y, and cross-shore and alongshore velocity scales U and V, we assume $L_x/L_y = U/V = \epsilon \ll 1$. We further assume $r/(|f|H)$ is of order ϵ, where H is a depth scale. With these assumptions (2.1) implies that the alongshore flow is geostrophic. Equation (2.2) becomes first-order in ϵ, so we expect that there will be places in which the contribution of bottom friction is comparable to those of pressure gradient or Coriolis force. With these assumptions,

following Csanady (1978), we can derive the well-known arrested topographic wave:

$$\eta_{1,2_{xx}} - \frac{1}{\kappa_{1,2}}\eta_{1,2_y} = 0, \tag{2.4}$$

where $\kappa_{1,2} = r/|f|s_{1,2}$, and $\eta_{1,2}$ and $s_{1,2}$ are the solutions and slopes on the shelf and the slope respectively. We choose coordinates so that the shelf and slope regions are defined by $-L \leqslant x \leqslant 0$ and $0 < x < \infty$ respectively. Density stratification is the most important of the effects neglected in the derivation of (2.4); see also §7 of Gawarkiewicz & Chapman (1991).

Chapman (1986) and Gawarkiewicz & Chapman (1991) used numerical methods to solve (2.1)–(2.3). They kept the friction term in (2.1), and derived a single elliptic equation in terms of a transport streamfunction, rather than the parabolic equation (2.4). Because of their parameter choices their results were similar to ours. They also included values of r that depended explicitly on x, but Chapman (1986) noted that the effect of variability of r was not significant.

We first derive solutions to (2.4) for the case investigated by Hill (1995), in which geostrophic inflow at the upstream boundary is confined to the slope, with no inflow on the shelf. A case in which inflow on the shelf is allowed is described in the Appendix. Following Hill (1995), we impose the boundary condition $\eta_{1_x}(-L, y) = 0$. We require the solution to be continuous and differentiable at the shelfbreak, i.e. $\eta_1(0, y) = \eta_2(0, y)$, $\eta_{1_x}(0, y) = \eta_{2_x}(0, y)$. We impose the inflow conditions specified by Hill, i.e.

$$\eta_1(x, 0) = 0, \tag{2.5}$$

$$\eta_2(x, 0) = \eta_0(\mathrm{e}^{-mx} - 1). \tag{2.6}$$

η_0 is the total change in sea level height across the inlet boundary and m defines the width of the inflow jet. The boundary conditions (2.5)–(2.6) lead to a well-posed problem, despite the fact that they violate the matching condition $\eta_{1x}(0, y) = \eta_{2x}(0, y)$, and in this idealized example the geostrophic velocity imposed at the upstream boundary is discontinuous. It is a feature of the solutions that the $\eta_{xx} \propto v_x$ will be discontinuous at the shelfbreak $x = 0$. This is clearly visible in the top panel of figure 3 of Chapman (1986). Gawarkiewicz & Chapman (1991), in their numerical study, used a bottom profile similar to ours, but with the slope made continuous by the addition of quadratic terms near the shelfbreak. Their domain also includes an abyssal plain beyond the slope, which is not present in our calculations. Like Chapman (1986), they imposed a discontinuous streamfunction at the upstream boundary, and in the upper panel of their figure 3, the cross-shelf profiles of the along-shelf velocity appear to be smooth.

Equation (2.4) can be solved by Laplace transforms (Carslaw & Jaeger 1959):

$$\mathscr{L}\eta_1 = A\cosh q_1(x + L), \tag{2.7}$$

$$\mathscr{L}\eta_2 = -\left(\frac{\eta_0}{\kappa_2 q_2^2} + \frac{\eta_0 \mathrm{e}^{-mx}}{\kappa_2(m^2 - q_2^2)}\right) + B\mathrm{e}^{-q_2 x}, \tag{2.8}$$

where $\mathscr{L}$ denotes the Laplace transform, $q_{1,2} = (s/\kappa_{1,2})^{1/2}$ and s is the transform variable. A and B are constants determined by the matching conditions:

$$A\cosh q_1 L = -\frac{\eta_0}{\kappa_2 q_2^2} - \frac{\eta_0}{\kappa_2(m^2 - q_2^2)} + B, \tag{2.9}$$

$$q_1 A \sinh q_1 L = \frac{m\eta_0}{\kappa_2(m^2 - q_2^2)} - q_2 B. \tag{2.10}$$

We can solve for A:

$$A = -\eta_0 \frac{m}{\kappa_2(m+q_2)q_2^2(\cosh q_1 L + \gamma \sinh q_1 L)} \tag{2.11}$$

where $\gamma = q_1/q_2 = (\kappa_2/\kappa_1)^{1/2}$.

The solution on the shelf is

$$\eta(x,y) = -\frac{\eta_0}{(1+\gamma)} \sum_{n=0}^{\infty} \left(-\frac{1-\gamma}{1+\gamma}\right)^n (F(2nL-x) + F(2(n+1)L+x)), \tag{2.12}$$

$$F = \operatorname{erfc}\left(\frac{x}{2(\kappa y)^{1/2}}\right) - \mathrm{e}^{hx+\kappa h^2 y}\operatorname{erfc}\left(\frac{x}{2(\kappa y)^{1/2}} + h(\kappa y)^{1/2}\right), \tag{2.13}$$

where $\kappa = \kappa_1$ and $h = \gamma m$. This is Hill's solution. The '$-$' sign appears here because the solution in this setup has to be negative for positive y.

The solution on the slope is more complicated. From (2.9) we have

$$B = A\cosh q_1 l + \frac{\eta_0}{\kappa_2 q_2^2} + \frac{\eta_0}{\kappa_2(m^2 - q_2^2)} \tag{2.14}$$

$$\equiv B^{(1)} + B^{(2)} + B^{(3)}. \tag{2.15}$$

The contribution to the solution in physical space of the term corresponding to $B^{(2)}$ is $\mathscr{L}^{-1}((\eta_0/s)\mathrm{e}^{-q_2 x}) = \eta_0 \operatorname{erfc}(x/2(\kappa_2 y)^{1/2})$. The solution defined by the second two terms of (2.14) along with the expression in parentheses in (2.8), i.e. everything but the contribution of $B^{(1)}\mathrm{e}^{-q_2 x}$, is given by

$$\begin{aligned}
&\mathscr{L}^{-1}((B^{(2)} + B^{(3)})\mathrm{e}^{-q_2 x}) + \mathscr{L}^{-1}\left(-\left(\frac{\eta_0}{\kappa_2 q_2^2} + \frac{\eta_0 \mathrm{e}^{-mx}}{\kappa_2(m^2 - q_2^2)}\right)\right) \\
&\quad = \eta_0(-1 + \operatorname{erfc}(x/2(\kappa_2 y)^{1/2})) + \eta_0 \mathrm{e}^{-mx}\mathrm{e}^{m^2\kappa_2 y} \\
&\qquad - \frac{\eta_0}{2}\mathrm{e}^{\kappa_2 m^2 y}\left(\mathrm{e}^{-mx}\operatorname{erfc}\left(\frac{x}{2(\kappa_2 y)^{1/2}} - m(\kappa_2 y)^{1/2}\right)\right. \\
&\qquad \left. + \mathrm{e}^{mx}\operatorname{erfc}\left(\frac{x}{2(\kappa_2 y)^{1/2}} + m(\kappa_2 y)^{1/2}\right)\right).
\end{aligned} \tag{2.16}$$

The contribution of $\mathscr{L}^{-1}B^{(1)}\mathrm{e}^{-q_2 x}$ to the solution in physical space is

$$\begin{aligned}
\mathscr{L}^{-1}(B^{(1)}\mathrm{e}^{-q_2 x}) = \frac{\eta_0}{1+\gamma} \sum_{n=0}^{\infty} &\left(-\frac{1-\gamma}{1+\gamma}\right)^n \\
&\times (F(2\gamma nL + x) + F(2\gamma(n+1)L + x))
\end{aligned} \tag{2.17}$$

where F is as in (2.13), with $\kappa = \kappa_2$ and $h = m$. So the full solution on the slope is the sum of the right-hand sides of (2.16) and (2.17).

3. Results

Our scale assumptions imply that the alongshore current v is geostrophically balanced, so $v = g\eta_x/f$ and u can be calculated from (2.2). Taking the curl of the momentum equations (2.1)–(2.2) we find

$$f(u_x + v_y) = -fw_z = -\left(\frac{rv}{h}\right)_x, \tag{3.1}$$

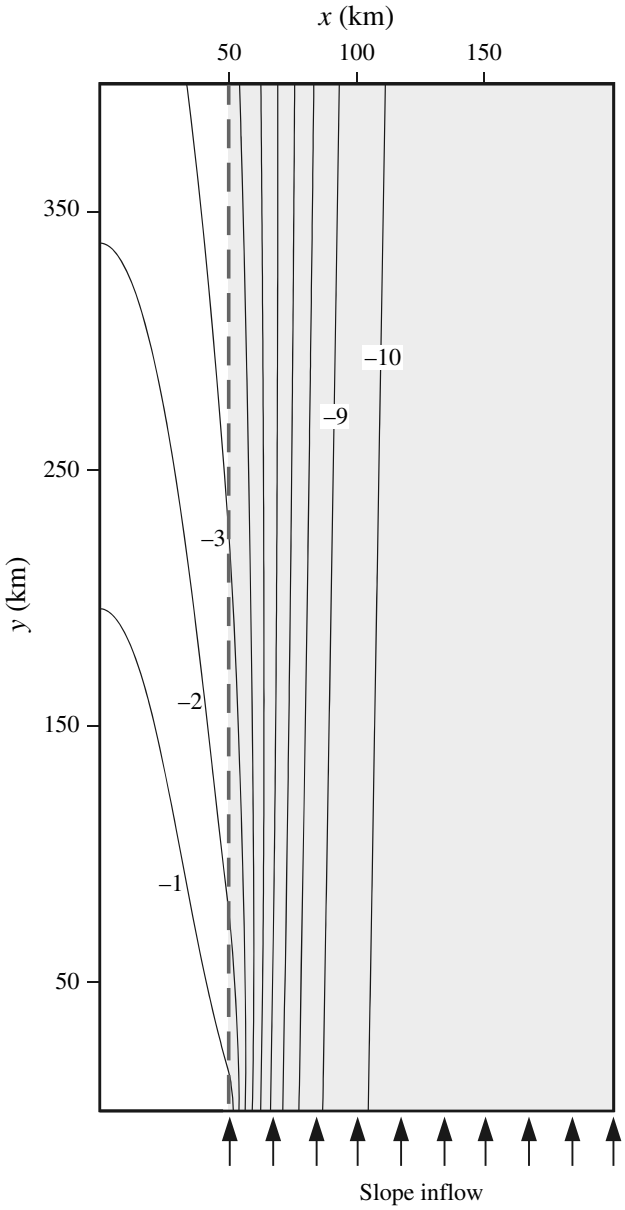

FIGURE 1. Height anomaly in centimetres from the solution to the arrested topographic wave. The inflow boundary condition is imposed at $y = 0$ (arrows). The shoreline boundary is at $x = 0$ and the model shelfbreak (dashed line) is 50 km offshore.

where we have neglected the friction term in (2.1). Integrating over the water column:

$$w(-h) = h(u_x + v_y) = \frac{-rv_x}{f} + \frac{rvh_x}{fh}. \tag{3.2}$$

We have used the three-dimensional continuity equation along with the assumption of vertical homogeneity and the fact that, at this level of approximation, the vertical velocity component w vanishes at the free surface. The two terms on the right-hand side of (3.2) represent the curl of the bottom stress and the lifting and lowering of water parcels by advection in the cross-shore direction by the ageostrophic velocity, cf. equation (4.9.32) of Pedlosky (1979).

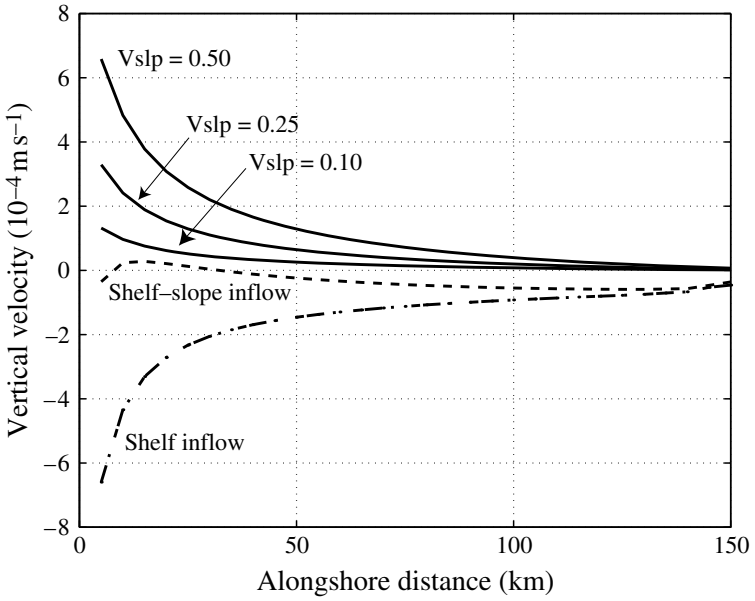

FIGURE 2. Vertical velocity sections. Maximum vertical velocity as a function of alongshore distance. Solid curves: no inflow on shelf, for selected values of maximum inflow velocity in m s^{-1}. $s_{1,2} = 2 \times 10^{-3}$, 3×10^{-2} respectively. Dashed curve: slope and shelf inflow maximum velocities equal 0.5 m s^{-1}. $\hat{r} = 2 \times 10^{-4}$. Dash-dotted curve: zero inflow on the slope, shelf inflow defined by (A 1), $\hat{r} = 2 \times 10^{-4}$.

Parameters were chosen to simulate the numerical experiments in MP08:

$$L = 50 \text{ km}, \tag{3.3}$$

$$\eta_0 = 0.1 \text{ m}, \tag{3.4}$$

$$m = (1/20\,000) \text{ m}^{-1}, \tag{3.5}$$

$$r = 0.001 \text{ m s}^{-1}. \tag{3.6}$$

L is the shelf width, equal to that chosen in MP08, m, which defines the width of the inflow jet, determines the peak inflow velocity (see (2.6)), chosen here to be about 0.5 m s^{-1}. The value of the linear drag coefficient r is typical of studies of this type, e.g. Chapman (1986) and Gawarkiewicz & Chapman (1991). We choose ranges of values for the bottom slopes s_1 and s_2 to illustrate parameter dependences. Nominal values of s_1 and s_2 are 2×10^{-3} and 3×10^{-2} respectively.

We first analyse the upwelling generated by a slope current, with zero inflow on the shelf. The term balance in the along-shelf momentum equation (2.2) is nearly geostrophic away from the shelf break. As in figure 5 of MP08, the contribution of friction takes the opposite sign to that of the pressure gradient inshore of the shelfbreak and the same sign offshore. In the analytic solution, all three terms in (2.2) are comparable in magnitude to corresponding quantities shown in figure 5 of MP08. The surface elevation of the analytical solution is characterized by a downstream spreading that induces both along-stream and cross-stream sea level gradients as shown in figure 1. Figure 2 shows the maximum vertical velocity at the shelfbreak as a function of alongshore distance and inflow magnitude. Upwelling decreases sharply downstream, but is still $O(10^{-4}$ m s$^{-1})$, similar in magnitude to values inferred from hydrographic data at the shelfbreak in the mid-Atlantic bight (e.g. Pickart 2000) and those found in coastal upwelling regimes, hundreds of kilometres downstream. As expected, shelfbreak upwelling increases with increasing bottom friction, since the

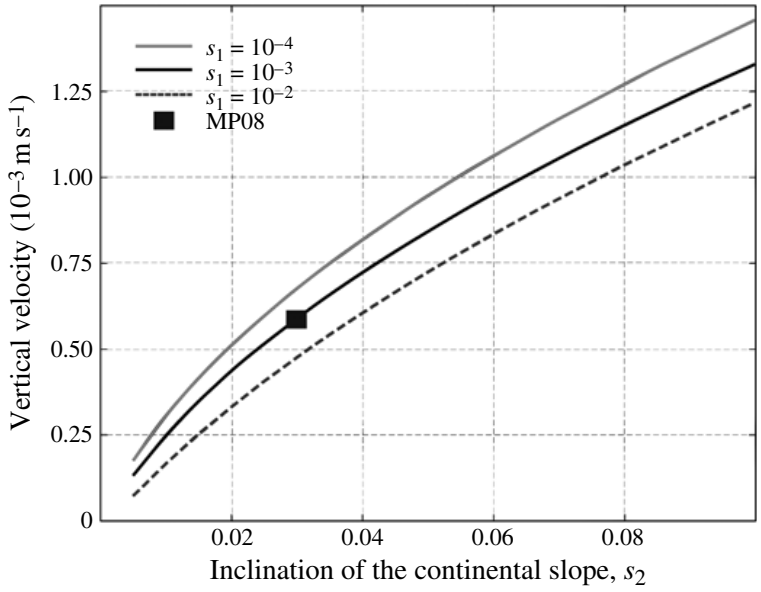

FIGURE 3. Maximum value of vertical velocity at the shelfbreak as a function of inclination of continental slope for selected values of the inclination of the shelf.

bottom drag coefficient amounts to parameterization of vertical velocity at the top of the bottom boundary layer.

Imposition of a shelf current decreases the magnitude of the shelfbreak upwelling (see dashed curve in figure 2), because the spreading of a shelf current into the steeper continental slope and consequently into a region with a smaller spreading rate generates mass convergence and hence downwelling. Thus, while a slope current generates shelfbreak upwelling, a shelf current generates shelfbreak downwelling, as shown by the dash-dotted curve in figure 2, consistent with MP08 as well as the results of Chapman (1986) and Gawarkiewicz & Chapman (1991).

The magnitude of the upwelling has different dependences on the inclination of the shelf and the continental slope (see figure 3). A steepening of the continental slope increases the magnitude of the upwelling but a steepening of the shelf decreases it, i.e. $w \propto s_2/s_1$. This reflects the fact that shelfbreak upwelling is produced by the difference between the spreading rates over the shelf and over the slope. Thus in the limiting case in which $s_1 = s_2$, i.e. no shelfbreak, there is no upwelling (MP08).

To facilitate comparison of our analytical solution to three-dimensional numerical results, we ran a series of numerical simulations using the barotropic model configuration described in MP08 with the parameters described above. Direct comparison of the maximum vertical velocities at $y = 20$ km for the experiment forced with a slope inflow of 0.5 m s^{-1} shows reasonable agreement between the numerical and analytical models (see figure 4). The numerical solution predicts smaller upwelling velocities with a maximum slightly displaced offshore of the shelfbreak. These details depend on the spatial resolution of the numerical model because it is difficult to represent the sharp change of slope used in the analytical solution. The numerical and analytical solutions show different parametric dependences, e.g. vertical velocities of the analytical solution are more sensitive to the magnitude of the bottom friction coefficient than those of the numerical simulation. The numerical results, nevertheless, show the same tendency to increase the vertical velocities with increasing bottom friction coefficient.

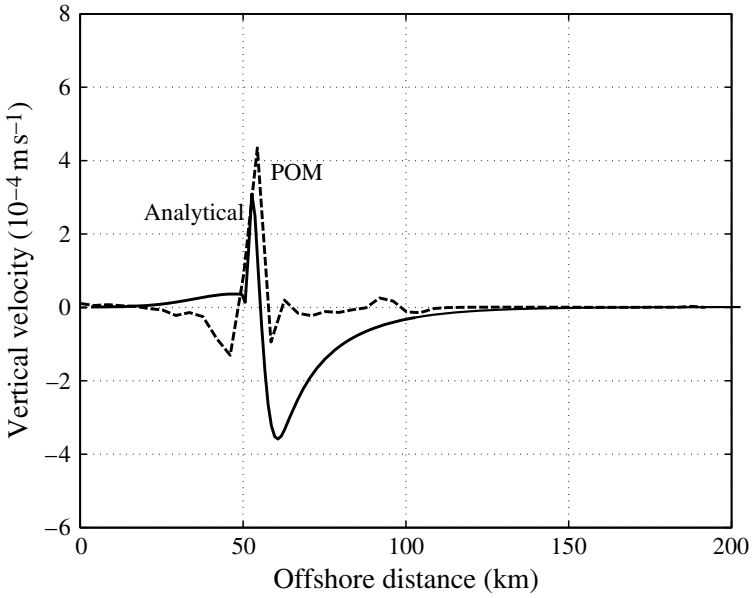

FIGURE 4. Vertical velocity as a function of cross-shore distance for the analytical solution with no flow on the shelf (solid line) and the numerical solution with no stratification (dashed line), 20 km from the upstream boundary. Shelfbreak is at $x = 50$ km.

4. Conclusions

MP08 suggested the arrested topographic wave as the physical mechanism for the shelfbreak upwelling of regions bounded by cyclonic currents. Our analytical solutions of the arrested topographic wave suggest strongly that this is, in fact, the case, as the arrested topographic wave accounts for much of the quantitative detail in the numerical simulations and is consistent with earlier work. Unlike wind-driven coastal upwelling systems, the upwelling produced by cyclonic currents can be sustained through the entire year, thus providing a continuous source of nutrients to the upper ocean. This should be particularly important in regions like Patagonia, where the nutrient rich waters of the Southern Ocean can be continuously fertilized by the steady flow of the Malvinas Current along the South American coast.

R.N.M. acknowledges the support of Office of Naval Research grant number 1010423, National Science Foundation award number 0934956-OCE and award NA08NES4400013 from the National Oceanic and Atmospheric Administration, US Department of Commerce, to the Cooperative Institute for Oceanographic Satellite Studies (CIOSS) and the Joint Center for Satellite Data Assimilation (JCSDA). The statements, findings, conclusions, and recommendations are those of the authors and do not necessarily reflect the views of the National Oceanic and Atmospheric Administration or the US Department of Commerce. R.P.M. acknowledges the support of the National Science Foundation through grants OCE-0726994 and OCE-0928348 and of NASA through grant NNX08AR40G. EDP acknowledges support from CONICET (PIP09-112-200801), ANPCYT (PICT08-1874), U. Nac. del Sur (24F044) and IAI grant CRN2076. The IAI is supported by the US NSF, grant GEO-045325. R.N.M. would like to thank E. Blayo and all of Team MOISE INRIA Rhône-Alpes for their hospitality during the time much of this work was done. We would also like to thank Professor R. Griffiths, as well as three anonymous reviewers, for helpful comments on earlier versions of the manuscript.

Appendix. Non-zero inflow on the shelf

Here we consider a mild generalization of the inflow condition (2.5) that includes poleward flow on the shelf:

$$\eta_1(x,0) = \frac{m\eta_0(\cosh(\hat{r}L) - \cosh(\hat{r}(x+L)))}{\hat{r}\sinh(\hat{r}L)}, \tag{A 1}$$

where the parameter $\hat{r}$ determines the shape of the surface anomaly on the shelf at inflow. The solution for the case with inflow conditions given by (A 1) and (2.6), is similar to (2.7) and (2.8):

$$\mathscr{L}\eta_1 = A_1\cosh q_1(x+L) + \frac{\eta_0 m}{\kappa_1\hat{r}\sinh(\hat{r}L)}\left(\frac{\cosh(\hat{r}L)}{q_1^2} + \frac{\cosh(\hat{r}(L+x))}{\hat{r}^2 - q_1^2}\right), \tag{A 2}$$

$$\mathscr{L}\eta_2 = -\left(\frac{\eta_0}{\kappa_2 q_2^2} + \frac{\eta_0 \mathrm{e}^{-mx}}{\kappa_2(m^2 - q_2^2)}\right) + B_1\mathrm{e}^{-q_2 x}. \tag{A 3}$$

A_1 and B_1 are determined by the matching conditions similar to (2.9) and (2.10):

$$A_1\cosh(q_1L) + \frac{\eta_0 m\coth(\hat{r}L)}{\kappa_1\hat{r}}\frac{\hat{r}^2}{q_1^2(\hat{r}^2 - q_1^2)} = -\frac{\eta_0}{\kappa_2}\frac{m^2}{q_2^2(m^2 - q_2^2)} + B_1, \tag{A 4}$$

$$q_1A_1\sinh q_1L + \frac{\eta_0 m}{\kappa_1(\hat{r}^2 - q_1^2)} = \frac{m\eta_0}{\kappa_2(m^2 - q_2^2)} - q_2B_1. \tag{A 5}$$

We then have

$$A_1 = A - \frac{\eta_0 m}{\cosh q_1L + \gamma\sinh q_1L}\left(\frac{1}{q_2\kappa_1(\hat{r}^2 - q_1^2)} + \frac{\hat{r}\coth(\hat{r}L)}{s(\hat{r}^2 - q_1^2)}\right) \tag{A 6}$$

where A is given by (2.11) and $\gamma = q_1/q_2 = (\kappa_2/\kappa_1)^{1/2}$ as before.

As in the case of the solution with no flow on the shelf, we make use of the identity

$$\frac{\cosh q_1(x+L)}{\cosh q_1L + \gamma\sinh q_1L} = \frac{1}{1+\gamma}\sum_{n=0}^{\infty}\left(-\frac{1-\gamma}{1+\gamma}\right)^n(\mathrm{e}^{-q_1(2Ln-x)} + \mathrm{e}^{-q_1(2L(n+1)+x)}). \tag{A 7}$$

The contribution of the first term in (A 2) to the full solution is the sum of the solution with zero inflow on the shelf (2.12) and two additional terms $A^{(2)}$ and $A^{(3)}$ given by

$$A^{(2)} = -\gamma\sum_{n=0}^{\infty}\left(-\frac{1-\gamma}{1+\gamma}\right)^n(F_2(2Ln-x) + F_2(2L(n+1)+x)), \tag{A 8}$$

$$A^{(3)} = \frac{\coth(\hat{r}L)}{\hat{r}}\sum_{n=0}^{\infty}\left(-\frac{1-\gamma}{1+\gamma}\right)^n(F_3(2Ln-x) + F_3(2L(n+1)+x)), \tag{A 9}$$

where

$$F_2 = \frac{1}{2\hat{r}}\left(\mathrm{e}^{-\hat{r}x}\mathrm{erfc}\left(\frac{x}{2(\kappa_1 y)^{1/2}} - \hat{r}(\kappa_1 y)^{1/2}\right)\right.$$
$$\left. - \mathrm{e}^{\hat{r}x}\mathrm{erfc}\left(\frac{x}{2(\kappa_1 y)^{1/2}} + \hat{r}(\kappa_1 y)^{1/2}\right)\right), \tag{A 10}$$

$$F_3 = \frac{1}{\hat{r}^2}\operatorname{erfc}\left(\frac{x}{2(\kappa_1 y)^{1/2}}\right) - \frac{\mathrm{e}^{\kappa_1\hat{r}^2 y}}{2\hat{r}^2}\left(\mathrm{e}^{-\hat{r}x}\operatorname{erfc}\left(\frac{x}{2(\kappa_1 y)^{1/2}} - \hat{r}(\kappa_1 y)^{1/2}\right)\right.$$
$$\left. + \mathrm{e}^{\hat{r}x}\operatorname{erfc}\left(\frac{x}{2(\kappa_1 y)^{1/2}} + \hat{r}(\kappa_1 y)^{1/2}\right)\right). \tag{A 11}$$

The contribution of the second term in (A 2) is

$$\mathscr{L}^{-1}\frac{\eta_0 m}{\kappa_1\hat{r}\sinh(\hat{r}L)}\left(\frac{\cosh(\hat{r}L)}{q_1^2} + \frac{\cosh(\hat{r}(L+x))}{\hat{r}^2 - q_1^2}\right)$$
$$= \frac{\eta_0 m}{\hat{r}\sinh(\hat{r}L)}(\cosh(\hat{r}L) - \mathrm{e}^{\kappa_1\hat{r}^2 y}\cosh(\hat{r}(L+x))). \tag{A 12}$$

For the slope, we may write as before

$$\eta_2 = \eta_0(\mathrm{e}^{\kappa_2 m^2 y}\mathrm{e}^{-mx} - 1) + \mathscr{L}^{-1}(B_1\mathrm{e}^{-q_2 x}). \tag{A 13}$$

From (A 5) we have

$$B_1 = \frac{m\eta_0}{q_2(m^2\kappa_2 - s)} - \frac{m\eta_0}{q_2(\hat{r}^2\kappa_1 - s)} - \gamma A_1\sinh(\gamma q_2 L). \tag{A 14}$$

We begin by computing $\mathscr{L}^{-1}(B_1\mathrm{e}^{-q_2 x})$:

$$\mathscr{L}^{-1}\frac{m\eta_0\mathrm{e}^{-q_2 x}}{q_2(m^2\kappa_2 - s)} = \frac{-\eta_0\mathrm{e}^{\kappa_2 m^2 y}}{2}\left(\mathrm{e}^{-mx}\operatorname{erfc}\left(\frac{x}{2(\kappa_2 y)^{1/2}} - m(\kappa_2 y)^{1/2}\right)\right.$$
$$\left. - \mathrm{e}^{mx}\operatorname{erfc}\left(\frac{x}{2(\kappa_2 y)^{1/2}} + m(\kappa_2 y)^{1/2}\right)\right), \tag{A 15}$$

$$\mathscr{L}^{-1}\frac{m\eta_0\mathrm{e}^{-q_2 x}}{q_2(\hat{r}^2\kappa_1 - s)} = \frac{-\eta_0\gamma\mathrm{e}^{\kappa_1\hat{r}^2 y}}{2\hat{r}}\left(\mathrm{e}^{-\hat{r}x/\gamma}\operatorname{erfc}\left(\frac{x}{2(\kappa_2 y)^{1/2}} - \hat{r}(\kappa_1 y)^{1/2}\right)\right.$$
$$\left. - \mathrm{e}^{\hat{r}x/\gamma}\operatorname{erfc}\left(\frac{x}{2(\kappa_2 y)^{1/2}} + \hat{r}(\kappa_1 y)^{1/2}\right)\right). \tag{A 16}$$

We must now calculate $\mathscr{L}^{-1}(\gamma A_1\sinh(\gamma q_2 L)\mathrm{e}^{-q_2 x})$. From (A 6) we have

$$\gamma A_1 = \gamma A - \frac{\gamma\eta_0 m}{\cosh(\gamma q_2 L) + \gamma\sinh(\gamma q_2 L)}\left(\frac{1}{q_2(\kappa_1\hat{r}^2 - s)} + \frac{\kappa_1\hat{r}\coth(\hat{r}L)}{s(\kappa_1\hat{r}^2 - s)}\right). \tag{A 17}$$

The inverse Laplace transforms are similar to those in the shelf calculation. Write $G_1 = F/m$, where F is as in (2.13) with $\kappa = \kappa_2$ and $h = m$,

$$G_2 = \mathscr{L}^{-1}\frac{\mathrm{e}^{-q_2 x}}{q_2(\kappa_1\hat{r}^2 - s)}$$
$$= \frac{-\gamma\mathrm{e}^{\kappa_1\hat{r}^2 y}}{2\hat{r}}\left(\mathrm{e}^{-\hat{r}x/\gamma}\operatorname{erfc}\left(\frac{x}{2(\kappa_2 y)^{1/2}} - \hat{r}(\kappa_1 y)^{1/2}\right)\right.$$
$$\left. - \mathrm{e}^{\hat{r}x/\gamma}\operatorname{erfc}\left(\frac{x}{2(\kappa_2 y)^{1/2}} + \hat{r}(\kappa_1 y)^{1/2}\right)\right), \tag{A 18}$$

$$G_3 = \kappa_1 \hat{r} \coth(\hat{r}L) \mathscr{L}^{-1} \left(\frac{\mathrm{e}^{-q_2 x}}{s} - \frac{\mathrm{e}^{-q_2 x}}{s - \kappa_1 \hat{r}^2} \right)$$
$$= \frac{\coth(\hat{r}L)}{\hat{r}} \mathrm{erfc} \left(\frac{x}{2(\kappa_2 y)^{1/2}} \right) - \frac{\coth(\hat{r}L)}{\hat{r}}$$
$$\times \frac{\mathrm{e}^{\kappa_1 \hat{r}^2 y}}{2} \left(\mathrm{e}^{-\hat{r}x/\gamma} \mathrm{erfc} \left(\frac{x}{2(\kappa_2 y)^{1/2}} - \hat{r}(\kappa_1 y)^{1/2} \right) \right.$$
$$\left. + \mathrm{e}^{\hat{r}x/\gamma} \mathrm{erfc} \left(\frac{x}{2(\kappa_2 y)^{1/2}} + \hat{r}(\kappa_1 y)^{1/2} \right) \right). \quad \text{(A 19)}$$

So finally, in physical space, we have

$$\mathscr{L}^{-1}(\gamma A_1 \sinh(\gamma q_2 L) \mathrm{e}^{-q_2 x}) = \frac{1}{1+\gamma} \sum_{j=1}^{3} \sum_{n=0}^{\infty} \left(-\frac{1-\gamma}{1+\gamma} \right)^n$$
$$\times (G_j(x + 2\gamma n L) - G_j(x + 2\gamma(n+1)L)). \quad \text{(A 20)}$$

REFERENCES

BLUMBERG, A. F. & MELLOR, G. L. 1987 A description of a three-dimensional coastal ocean circulation model. In *Three-Dimensional Coastal Ocean Models* (ed. N. Heaps), *Coastal Estuarine Science*, vol. 4. pp. 1–16. Am. Geophys. Union.

CARSLAW, H. S. & JAEGER, J. C. 1959 *Conduction of Heat in Solids*. Oxford University Press.

CHAPMAN, D. C. 1986 A simple model of the formation and maintenance of the shelf/slope front in the Middle Atlantic Bight. *J. Phys. Oceanogr.* **16**, 1273–1279.

CSANADY, G. T. 1978 The arrested topographic wave. *J. Phys. Oceanogr.* **8**, 47–62.

GAWARKIEWICZ, G. & CHAPMAN, D. C. 1991 Formation and maintenance of shelfbreak fronts in an unstratified flow. *J. Phys. Oceanogr.* **21**, 1225–1239.

HILL, A. E. 1995 Leakage of barotropic slope current onto the continental shelf. *J. Phys. Oceanogr.* **25**, 1617–1621.

MATANO, R. P. & PALMA, E. D. 2008 On the upwelling of downwelling currents. *J. Phys. Oceanogr.* **38**, 2482–2500.

PEDLOSKY, J. 1979 *Geophysical Fluid Dynamics*. Springer.

PICKART, R. S. 2000 Bottom boundary layer structure and detachment in the shelfbreak jet of the Middle Atlantic Bight. *J. Phys. Oceanogr.* **30**, 2668–2686.